# DESIGN AND DYNAMIC OPTIMIZATION OF A TRISTABLE X-RAY ATTENUATOR MECHANISM FOR THE STIX INSTRUMENT

**M. Lai [(1)], F. Rottmeier [(1)], M. Humphries [(2)], L. Blecha[(1)]**

[(1)] *Almatech, space and naval engineering, EPFL- Innovation Park, 1015 Lausanne, Switzerland,*
*Emails: marco.lai@almatech.ch, fabrice.rottmeier@almatech.ch, luc.blecha@almatech.ch*
[(2)]*SpaceMech, 36 Charlton Gardens, Westbury-on-Trym, Bristol BS10 6LX, United Kindgdom,*
*Email: martin.humphries@spacemech.co.uk*

## ABSTRACT

The STIX (Spectrometer/Telescope for Imaging X-rays) instrument on the ESA Solar Orbiter satellite is designed to study the Sunrays emissions. The wide energy range of incident X-ray fluxes, expected during the solar flares, requires the incorporation of a moveable X-ray attenuator covering and uncovering the instrument detectors depending on X-ray fluxes intensity.

In the frame of the STIX Detector Module Prime Contract with ESA, Almatech has designed an attenuator mechanism provided with 2 end-strokes and 1 neutral-mid-stroke stable positions. In particular, the two stable end-stroke positions avoid the use of a dedicated launch-lock device to reduce complexity, lower the total mass while increasing the system reliability, all in the same time.

Flexures as well as end-position switches are used as accelerator/decelerator devices in the mechanism. A cam-shaped switch trigger design allows the optimization of their dynamic contributions in the system.

This article first presents the design of the STIX Attenuator Mechanism and then focuses on presenting the optimization of its dynamic response that plays a major role in the limitation of exported force, micro vibrations and torque to the spacecraft on one hand, as well as on the required actuation power on the other hand.

## MISSION AND INSTRUMENT DESCRIPTION

Solar Orbiter is the first of the two selected M-Class ESA missions. Solar Orbiter (SOLO) will be launched by NASA in October 2018.

The mission overall goal is to produce images of the Sun at an unprecedented resolution and perform closest ever in-situ measurements. SOLO destination is an elliptical orbit around the Sun with perihelion as low as 0.28 AU.

Ten instruments will be accommodated in the spacecraft, 6 of which are remote-sensing instruments and 4 are in-situ instruments.

Due to its proximity to the sun, Solar Orbiter will be subjected to severe thermal environment. To protect the instrument from the solar flux, a large heat shield is positioned on the spacecraft side facing the sun. Holes are accommodated in the heat shield to allow direct sun observation.

Among the 6 remote sensing instruments, the STIX instrument provides imaging spectroscopy of solar thermal and non-thermal X-ray emission from ~4 to 150 keV with spectral resolution as high as 1 keV FWHM and unprecedented sensitivity and spatial resolution (near perihelion). STIX plays an important role in enabling Solar Orbiter to achieve two of its major science goals

(1) Determining the magnetic connection of the Solar Orbiter back to the Sun

(2) Understanding the acceleration of electrons at the Sun and their transport into interplanetary space.

The remote-sensing X-ray measurements made with STIX will determine the intensity, spectrum, timing, and location of accelerated electrons near the Sun.

STIX is based on a Fourier-transform imaging technique. It consists of three, mechanically separate modules:

- A pair of X-ray windows and a heat shield feed-through;
- An Imager Module with 32 X-ray sub-collimators plus an optical aspect system;
- A Detector Electronics Module (DEM)

The Detector Electronics Module hosts the 32 X-ray detectors and the Attenuator mechanism which is the object of the present paper.
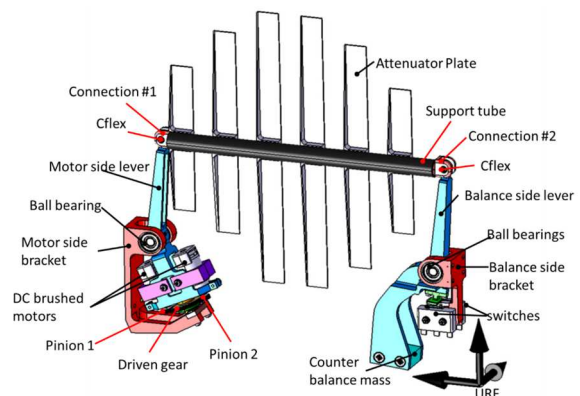


*Figure 1 : Overview of the ATM mechanism*

## MECHANISM DESCRIPTION

The Attenuator mechanism design is illustrated in *Figure 1* together with the labelling of its principal components. The movement of the attenuator is achieved by a parallelogram-like structure which is composed of the balance side lever, the support tube and the motor side

lever. Such structure ensures a global translation of the attenuator plate assembly, fixed at the end of the two side levers, while the driving movement of the levers is rotational. The amplitude of the movement of the levers is of $\alpha=\pm5.52°$ degrees with respect to the vertical direction. This in plane rotational angle is achieved by transforming the pinion rotation of each motor in angular motion of the mechanism. The transformation is obtained by means of a reaction block and an eccentric guiding pin mounted on the driven gear.

The movement of the guiding pin is illustrated in the 3 main positions reported in *Figure 3*. The presented detailed view of the drive system is shown from the bottom with respect to the drawing of *Figure 2*.
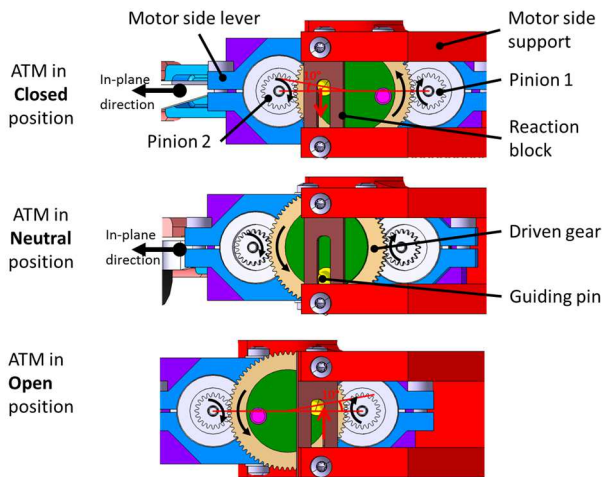


*Figure 3 : Driving principle of the motor concept (ATM in plane movement from closed position to open position).*

The guiding pin, eccentric w.r.t. the driven gear axis, is forced to exit its stable position (position within angle of 10° degrees) by increasing the actuation torque. Then, the guiding pin slides along the left side of the guiding slit of the reaction block (see *Figure 3*) to reach the ATM neutral position.

The neutral position is stable thanks to the counter-acting Cflex design that results in the equilibrium of moments at this location. The movement is then continued with the pin sliding along the right side of the guiding slit of the reaction bloc such to reach the other stable position and lock the mechanism. The two stable end positions of the attenuator mechanism, as viewed in the line of sight of the instrument, are presented in the global view of the STIX Detector Module in *Figure 4*. In addition, this figure indicate the location of the detail views provided in *Figure 3* and *Figure 5*.

The pivoting elements of the mechanism are 2 Cflex elements and 2 deep grove ball bearings (see *Figure 1*).

The purpose of the ATM is to displace a set of X-Ray attenuating blades in front of the 32 detectors within a position accuracy of ±0.1mm over a travel distance of ~11.5 mm. In the closed position, the attenuation material is positioned in the field of view of the detector and thus attenuates the incoming X-rays. In the open position, the attenuation material is away from the field of view of the detector and no attenuation is provided. A global view of the attenuator mechanism with respect to the detector module, and in particular w.r.t. the 32 X-ray detectors is shown in *Figure 4*.
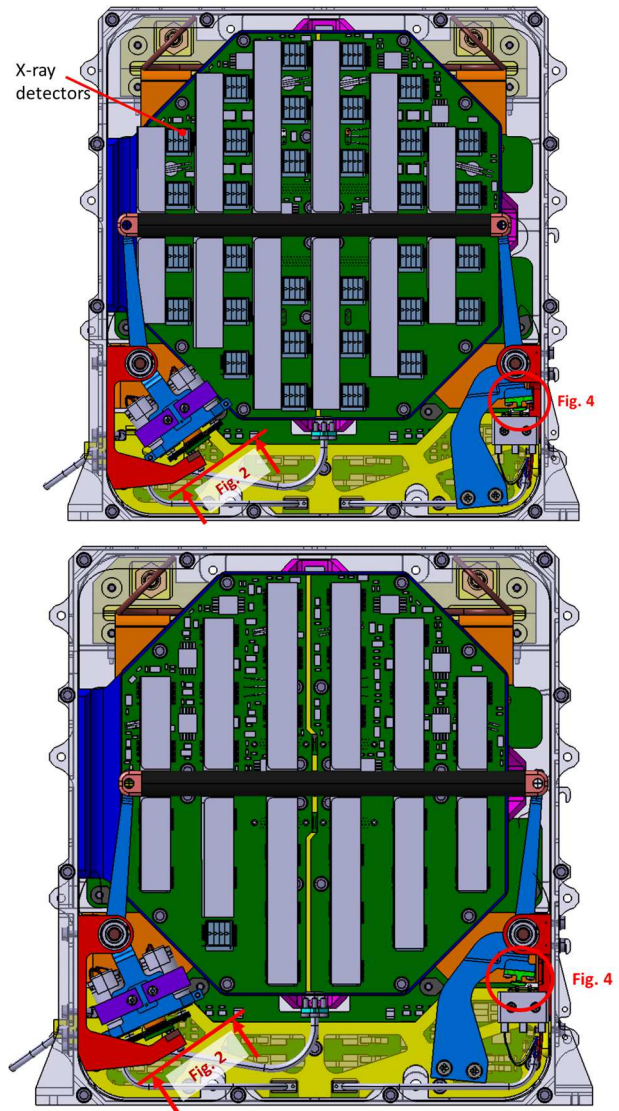


*Figure 4 : Global view of the Attenuator mechanism inside the STIX Detector Module in open (up) and closed (down) configurations.*

The COG of the moving parts is set to be located on the line connecting the two principal hinges of the mechanism, which are identified by the ball bearing axes linking the 2 support brackets to the levers. This design configuration results in the minimization of the exported forces. To achieve a well-balanced ATM, a counterbalance mass is then added to the switch side lever. The counterbalance mass is proportional to the mass of the ATM moving part. Therefore, the mass of the moving parts is highly optimized, to further limit the

related counterbalance mass in the same time. While the design mass is estimated on the basis of 3D modelling of the mechanism, uncertainties on final mass and CoG location resulted in the decision to balance each flight mechanism individually.

Such well-balanced mechanism minimizes exported forces and makes unnecessary a launch locking device that represents important risks of inoperative mechanism in case of failure. In addition, avoiding launch lock also simplifies the control electronics, and therefore saves mass and mitigates failure risks of electronic components.

## DESIGN DRIVERS AND PHILOSOPHY

The STIX Attenuator Mechanism was driven by a set of objectives detailed hereafter:

1. Mass: the total mass budget for the mechanism was very tight: 200gr. Therefore, the design must be as light as possible. The approach followed during the mechanism development was to simplify the design keeping at minimum the number of parts and components, and to identify the electrical parts such as actuators, switches, locking devices that are the lightest possible while maintaining sufficient functional margin.

2. Motorization margin, reliability and redundancy. The actuation principles identified for the attenuator mechanism were based on elements with high reliability and significant space heritage. In addition, sufficient motorization margin was provided for each actuator by design. Redundancy is implemented on the actuation drive that further allows the control of both actuators simultaneously in case of failure.

3. Control electronics: the driving and sensor elements are chosen to keep associated control electronics as simple as possible. The design is also developed to simplify as much as possible the control algorithm.

4. Structural strength and dynamic behavior: The design is such to maximize the strength and the stiffness of the structure while minimizing its mass. This is a usual constrain for space structures.

## MECHANISM KEY FEATURES

The following feature could be identified as key design parameter in order to fulfil the demanding specifications:

- The main hinges are ball bearing to provide sufficient stiffness, motor torque margin and smooth movement avoiding shock and large exported forces.
- The mechanism includes flex pivots as the rotation angle is small. This avoids unpredictable friction, wears debris and ensures reliability and repeatability of the movement. The flex pivots provide back

driving force that is necessary to lock the mechanism on the end-positions.

- The architecture of the mechanism ensures also 3 stable positions: in ATM open, in ATM closed, and in ATM intermediate stable position.
- The mechanism includes two micro switches to determine open/close position status
- The mechanism is powered by two brushed DC motors assembled in mirrored configuration. One single motor is capable of activating the mechanism with large margins. The implemented configuration ensures in first place redundancy, since the second motor can replace the first one in activating the mechanism. Secondly, it allows for the possibility to deliver double the necessary torque, in case of unexpected mechanism performance deterioration, when two motors are powered simultaneously.

## MODELS EVOLUTION AND LESSONS LEARNED.

The evolution of the mechanism design was minimal through the project phases, underlining the quality of the selected baseline concept.

The PDR model was conceived with the 4 hinges all implemented with Cflex bearings. Two double Cflex on the upper hinges, and a pair of single Cflex on each of the lower hinges. No ball bearings were initially used.

The analysis and breadboard testing at PDR level already showed good results, although some improvements were necessary. In particular, the random FE analysis of the mechanism highlighted negative margin of safety at the lower pairs of Cflex. In addition, the maximal acceleration developed during the movement generated unacceptable exported forces. Moreover, the torque necessary to complete the movement was linked to the resistive torque generated during the triggering of the end-position switch. The non optimized shape of the trigger element caused undesired loss and reduced the motorization margin of each motor.

Following the identified improvement paths, the ATM design was modified as reported in *Figure 1* for the CDR. In particular, the replacement of the lower Cflex hinges by ball bearings were implemented in order to:

- reduce the mechanism resistive torque
- reduce the initial deceleration
- reduce the locking force at each stable position
- allow for positive margins during the random vibration

and the optimization of the trigger shape was introduced in order to:

- reduce the required torque
- reduce maximum mechanism acceleration since the switches are used as system decelerators during the movement

## MECHANISM OPTIMIZATION

The optimization was conducted by implementing a pure dynamic model of the mechanism, considering all the components as rigid body elements, into MSC Adams.

## DYNAMIC MODEL DESCRIPTION

The model explicitly considers all the contribution to the resistive torque due to frictional forces in rotating elements:

- ball bearings
- journal bearings supporting the gear assembly and all the sliding contacts between
  - the gears
  - the trigger and the switch heads
  - the reaction block and the guiding pin.

Only the service condition in which one single motor is powering the movement has been simulated. In this nominal configuration, the first motor is powered in current control mode and thus a representative torque profile is prescribed on the motor 1 pinion. The other motor is model as an additional load, since it does not actively participate to the mechanism movement. Its contribution is modelled as an imposed additional resistive torque counteracting the torque provided by the first motor.

The Cflex are modelled as rotational spring elements with zero torque produced when the mechanism is in neutral position. On the other hand, when the mechanism is at either end stop positions, both Cflexes provide a counteracting torque willing to re-establish the neutral configuration. This moment contributes to the locking force of the mechanism into the end positions configurations.

The force generated by the switches during their activation is due to the switch heads being installed on a cantilever beam which is simulated by a linear spring whose constant was determined experimentally.

## TRIGGER SHAPE OPTIMIZATION

The optimization involved mainly the shape of the trigger whose evolution is reported in *Figure 5*. The optimization started aiming at reducing the slope of the surfaces impacting on the two switches heads. The next step was to introduce the constraint of a complete switch activation and the constraint of a single point of contact of the trigger with the switch heads when each of the 2 end positions are met. The latter constraint was necessary to avoid any possible ambiguity in the analysis of the signal gathered by the switches. The optimized shape presents a twofold advantage. Firstly, the obtained profile is the most congruent possible with respect to the movement of the trigger over the switch heads. Thus producing the lowest resistive torque while ensuring complete switch activation.

Secondly, the extension of the trigger width allows it to come in contact with the opposite switch head relatively early during the movement. When this contact is established a reaction force is generated which is directly dependent on the friction coefficient between the contact surfaces and the spring constant of the blade mount of the switch head. The momentum associated to this reaction force counteracts the torque applied by the motor, thus reducing the acceleration of the movement.
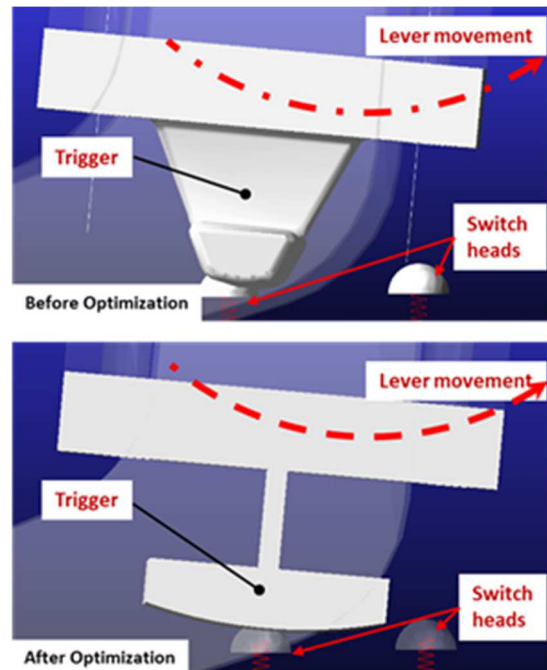


*Figure 5 : trigger shape: before optimization (up), after optimization (down).*

## OPTIMIZATION RESULTS

The results of the optimization are evaluated in the subsequent sections by considering the following characteristics:

- resistive torque generated by the mechanism as function of the drive gear angle for the optimized and not optimized trigger shape
- current drawn by the motor pins during the test on the ATM in original configuration and in the optimized version.
- Acceleration developed by the mobile parts during movement.

## RESISTIVE TORQUE EVOLUTION

The quality of the optimization is primarily evaluated considering the evolution of the resistive torque generated by the mechanism while an imposed rotation on the activating pinion is prescribed. In this simulation the pinion rotates at 60°/second. The comparison of the resistive torque developed when the two versions of the trigger are considered is reported in *Figure 6* as function of the rotation angle of the driven gear. The beginning of the movement is identified by $\beta=-100°$ and the end of the movement by $\beta=100°$.
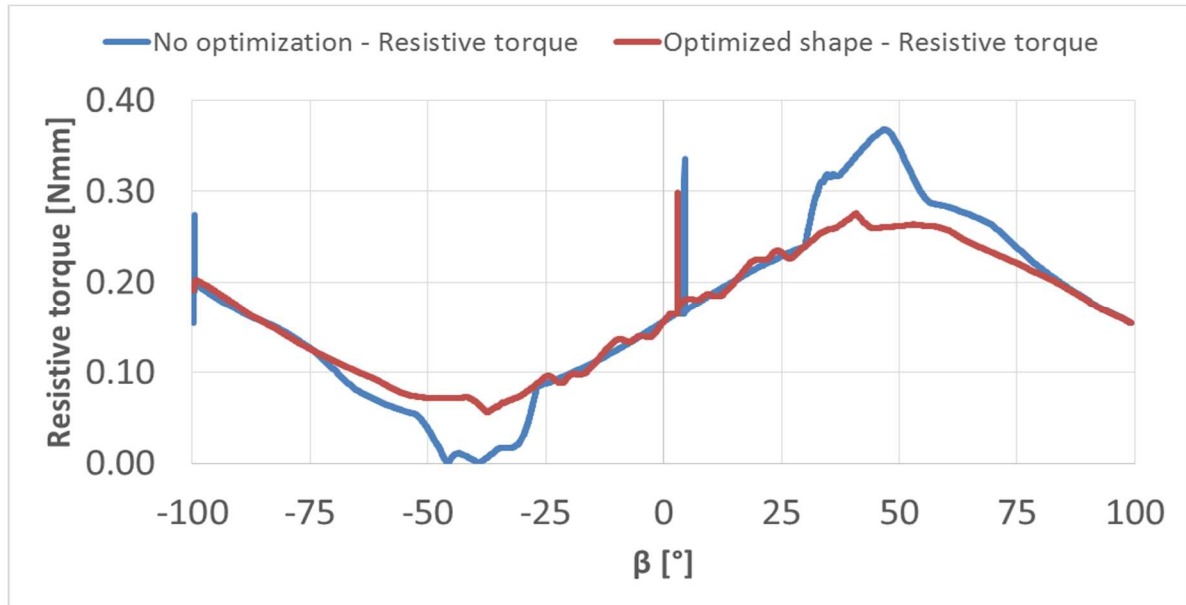
*Figure 6 : Resistive torque evolution as function of the driven gear angle
for the optimized and non-optimized trigger shape.*

At the beginning of the movement, both resistive torques decrease because of the idling moment of the Cflexes as well as the force applied by the switch that is already in contact on the trigger cam. However, in the case of the initial and non-optimized trigger shape, it can be seen that the resistive torque decreases rapidly and goes to zero for $-50° \leq \beta \leq -25°$. This behavior is due to the earlier loss of contact between the first switch head and the non-optimized trigger shape. In fact, in the original configuration, the reduced width of the trigger allowed for a free time of flight before encountering the second switch head.

If the optimized shape is considered, the corresponding resistive torque is always greater than zero since the trigger, before leaving completely the first switch head, run in contact with the second one, which generates the additional resistive torque. This configuration allows for a continuous and progressive braking function that gradually reduces the acceleration of the mechanism.

## MOTOR CURRENT EVOLUTION

The test on the ATM initial configuration were conducted in voltage control and, to allow a verification of the increase in performances between the two versions of the mechanism, the same test was performed after the trigger optimization.

It must be said, as explained earlier, that the differences between the initial version of the mechanism and the optimized one are not limited to the shape of the trigger optimization but involves also the introduction of the ball bearing at the lower mechanism hinges.

The current drawn by the motor during the two tests is reported in *Figure 7* for the opening and closing movement. The same voltage ramp is imposed for both tests, and the sign is reversed in order to reverse the mechanism movement. It can be noticed in *Figure 7* that the current evolution is linear before and after the movement because of the motor acting as pure resistor in this conditions. When the movement takes place the current is reduced in absolute value because of the generation of the electromotive force. From *Figure 7* it is also noticeable that the beginning of the current drop is massively reduced after the optimization process.

In particular, the mechanism optimization resulted in a drastic decrease of the current consumption of 11 times (~220 mA before the optimization and of ~20mA after the optimization). In addition, the current consumption at the end of the movement is reduced by more the 3 times (~240mA w.r.t. ~85mA).

Considering the curves relative to the closing phase the same behavior is qualitatively conserved. However, the increase of performance is reduced due to the slight asymmetric behavior of the mechanism during the closing and opening phase.

Moreover, it can also be noticed that the movement time is shorter before the optimization which indicates a greater acceleration of the mechanism as confirmed by the dynamic analysis.

## EXPORTED FORCES

The calculation of the exported forces was done on the basis of the measured accelerations at the support tube axis. In fact, during the activation the displacement of the tube axis was determined by means of a laser sensor pointing at the part labelled "connection 2" in *Figure 1*.
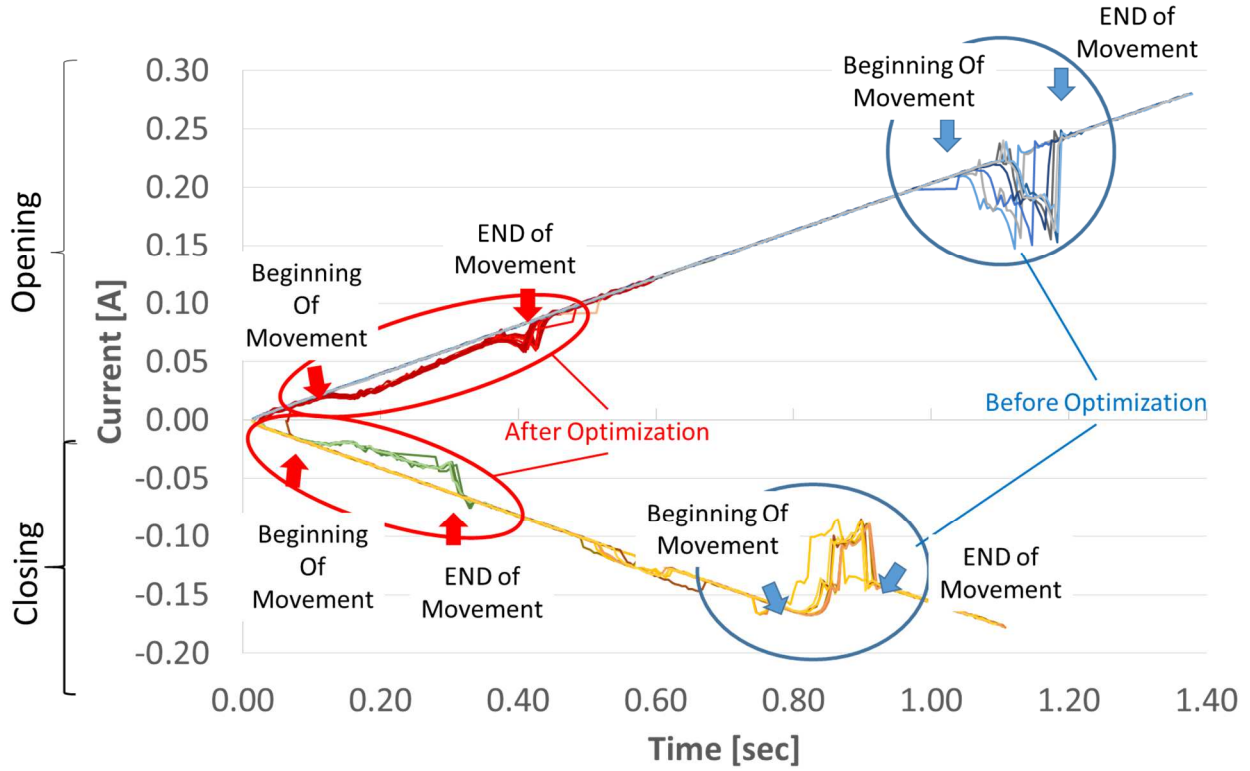
*Figure 7 : current drawn by the motor during mechanism activation before and after optimization. 10 curves for each movement and each mechanism version are reported: closing phase before optimization (yellow curves), opening phase before optimization (blue curves), opening phase after optimization (red curves), closing phase after optimization (green curves).*

The time-based data was smoothened using a moving average technique and then derived twice in order to calculate the acceleration at that location.

The comparison of the results for the optimized and non-optimized mechanism are reported in *Figure 8*. It can therein be seen that the positive acceleration peaks is decreased by a factor of ~6.3 (8865 mm/s$^2$ and 1400 mm/s$^2$ for the non-optimized and optimized mechanism, respectively).
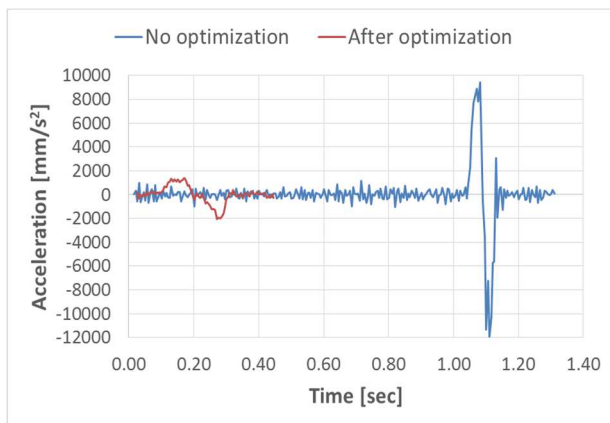


*Figure 8 : Acceleration at the tube support axis before and after the optimization.*

Moreover, the peak related to the deceleration part of the movement is decreased by a factor of ~5.6 (11492 mm/s$^2$ w.r.t. 2053 mm/s$^2$.

The value of the exported force can be calculated using Eq. 1.

$$F_{exp} = acc_{tube} * L_{COG}/L_{tube} * m_{mobile\ parts} \qquad Eq.\ (1)$$

Where

- $acc_{tube}$ is the measured acceleration
- $L_{COG}$ is the distance of the COG from the ball bearing axis
- $L_{tube}$ is the distance of the support tube axis from the ball bearing axis
- $m_{mobile\ parts}$ is the total mass of the mobile parts.

The ratio $L_{COG}/L_{tube}$ gives an estimation of the balance state achieved by the mechanism assembly. A perfectly balanced mechanism will have a ratio of 0 thus null exported forces. Here it is assumed that the COG is misplaced by a maximum of 12mm from the ball bearing axis. This value corresponds to a $L_{COG}/L_{tube}=0.2$.

Under this assumption, the peak of exported forces at S/C interface are 0.222N versus 0.035N in the case of positive acceleration, before and after optimization respectively. This corresponds to a total reduction of 84 % of the peak

exported forces. In the deceleration case the peak forces are 0.287 N and 0.051N, before and after optimization, respectively. This corresponds to a total reduction of 82% of the peak exported forces. The maximum force developed at the S/C interface are now well below the required value of 0.1N.

**CONCLUSIONS**

The developed STIX Attenuator Mechanism design demonstrated to be compliant to all its requirements, following a design optimization of its dynamic behavior. Multi-body dynamic simulations allowed to identify key parameters in the dynamic response of the STIX Attenuator Mechanism such to predict design enhancements impacts and optimize its design efficiently.

The presented design optimization allowed an effective reduction of the exported forces such to bring it to its compliance with significant margins. Additionally, the needed actuation torque has been significantly reduced, thus reducing the required power consumption for activation as well increasing the motorization margins.

The optimization of the use of the switches as dynamic braking element contributed efficiently to the reduction of the exported forces although a significant part of the improvement has to be attributed to the replacement of Cflexes by ball bearings at the lower hinge location.